nature photonics

ARTICLES

PUBLISHED ONLINE: 13 MAY 2012 | DOI: 10.1038/NPHOTON.2012.104

Photovoltaic retinal prosthesis with high pixel density

Keith Mathieson[1,4†], James Loudin[1,2†*], Georges Goetz[1,3], Philip Huie[1,2], Lele Wang[3], Theodore I. Kamins[3], Ludwig Galambos[3], Richard Smith[4], James S. Harris[3], Alexander Sher[4] and Daniel Palanker[1,2]

Retinal degenerative diseases lead to blindness due to loss of the 'image capturing' photoreceptors, while neurons in the 'image-processing' inner retinal layers are relatively well preserved. Electronic retinal prostheses seek to restore sight by electrically stimulating the surviving neurons. Most implants are powered through inductive coils, requiring complex surgical methods to implant the coil-decoder-cable-array systems that deliver energy to stimulating electrodes via intraocular cables. We present a photovoltaic subretinal prosthesis, in which silicon photodiodes in each pixel receive power and data directly through pulsed near-infrared illumination and electrically stimulate neurons. Stimulation is produced in normal and degenerate rat retinas, with pulse durations of 0.5–4 ms, and threshold peak irradiances of 0.2–10 mW mm^{-2}, two orders of magnitude below the ocular safety limit. Neural responses were elicited by illuminating a single 70 μm bipolar pixel, demonstrating the possibility of a fully integrated photovoltaic retinal prosthesis with high pixel density.

Retinal degenerative diseases such as age-related macular degeneration (one of the leading causes of blindness in the developed world[1]) and retinitis pigmentosa (the leading cause of inherited blindness[2]) lead to the loss of photoreceptors, but the inner retinal neurons, to a large extent, survive[3–5]. Electrical activation of these neurons can produce visual percepts (phosphenes), thereby providing an alternative route to visual information, raising hope for the restoration of sight to the blind.

Recent clinical trials with electrode arrays implanted either epiretinally (facing the ganglion cell side) or subretinally (facing the photoreceptor side) have restored visual acuity on the order of 20/1,200 to subjects blinded by retinal degeneration[6,7]. Although this serves as an important proof of concept with clinically useful implications, existing retinal prosthesis designs suffer from a number of shortcomings. Many implants deliver stimulation signals using serial telemetry and distribute them over the electrode array via an intraocular cable[6], a design that is difficult to scale to the large numbers of densely packed microelectrodes required for higher visual acuity. Additionally, the bulky intraocular receiving and processing electronics makes surgery more complex and increases the probability of undesirable side effects[8]. Finally, retinal stimulation patterns in such systems are fully determined by images captured by the external camera, regardless of eye orientation. Thus, patients cannot use natural eye movements to scan the visual scene, which is a very important feature of normal visual perception. Devices with photosensitive pixels (such as that from Retina Implant AG[7]) largely overcome the scalability limitation and make use of natural eye movements, but still depend on external power delivered via radiofrequency coils and a trans-scleral cable. Our design overcomes these problems by using microfabricated arrays of photodiodes driven photovoltaically. It has been shown that subretinal photovoltaic arrays can stimulate the retina *in vivo* and provide signals to the central visual system when illuminated by an intense full-field near-infrared (NIR) flash[9]. However, to date, all photosensitive electronic systems have been either too weak to produce patterned retinal stimulation[10] or have required a separate power source to amplify the ambient optical signals[7].

Here, we describe a photovoltaic retinal prosthesis system design in which video goggles deliver both power and visual information directly to each pixel through pulsed NIR illumination, eliminating the need for complex electronics and wiring schemes, and preserving the natural link between image perception and eye movement. We demonstrate the plausibility of this design through successful *in vitro* stimulation of healthy and degenerate[11] rat retina with NIR light intensities at least two orders of magnitude below the ocular safety limit. We also demonstrate the possibility of high-resolution stimulation with retinal responses elicited by a single 70 μm bipolar pixel containing a 20 μm active electrode and a local concentric return electrode for improved isolation from neighbouring pixels.

System design

The photovoltaic retinal prosthetic system is shown in Fig. 1. A pocket computer processes images captured by a miniature video camera. A near-to-eye projection system (similar to conventional video goggles) projects these images into the eye and onto a photodiode array using pulsed NIR (880–915 nm) light[12,13]. Photodiodes in each pixel of the subretinal array convert this light into pulsed photocurrent. Iridium oxide electrodes deliver these stimulating pulses to the retina, targeting primarily the surviving cells in the inner nuclear layer (INL). Although an epiretinal photovoltaic stimulation design is also feasible, subretinal stimulation of the graded-response inner retinal neurons may provide some advantages. For example, mediation by non-spiking neurons may result in a more natural conversion of the pulsed spatiotemporal

[1]Hansen Experimental Physics Laboratory, 452 Lomita Mall, Stanford University, Stanford, California 94305-4085, USA, [2]Department of Ophthalmology, The Byers Eye Institute at Stanford University, 2452 Watson Court, Palo Alto, California 94303, USA, [3]Department of Electrical Engineering, Stanford University, 350 Serra Mall, Stanford, California 94305-9505, USA, [4]Santa Cruz Institute for Particle Physics, University of California, Santa Cruz, 1156 High Street, Santa Cruz, California 95064, USA; †These authors contributed equally to the study and share primary authorship.
*e-mail: jim.loudin@alumni.stanford.edu

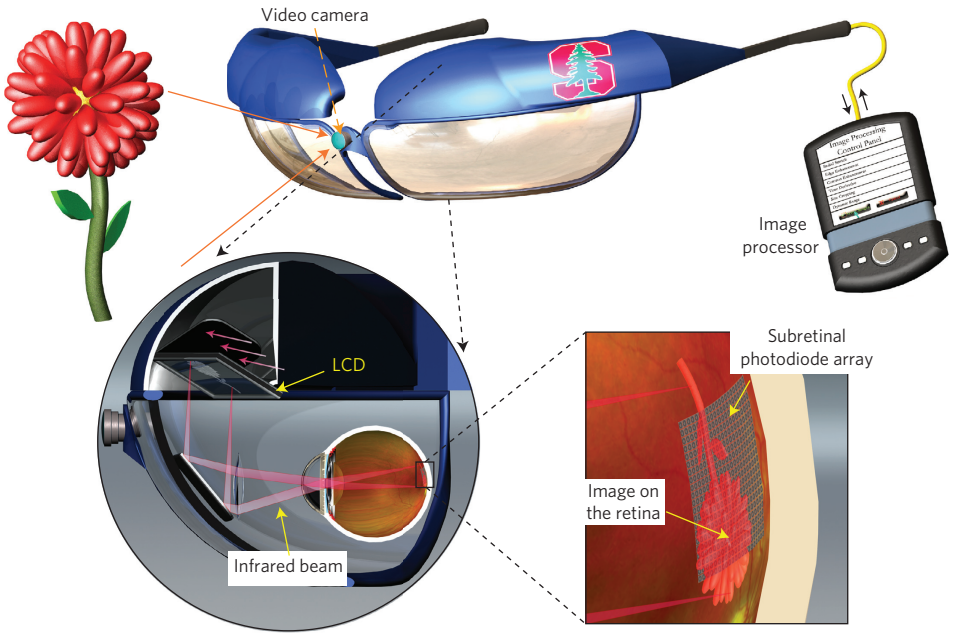

Figure 1 | Simplified system diagram. A portable computer processes video images captured by a head-mounted camera. Video goggles then project these images onto the retina using pulsed infrared (880–915 nm) illumination. Finally, pixels in the subretinal photodiode array convert this light into local stimulation currents.

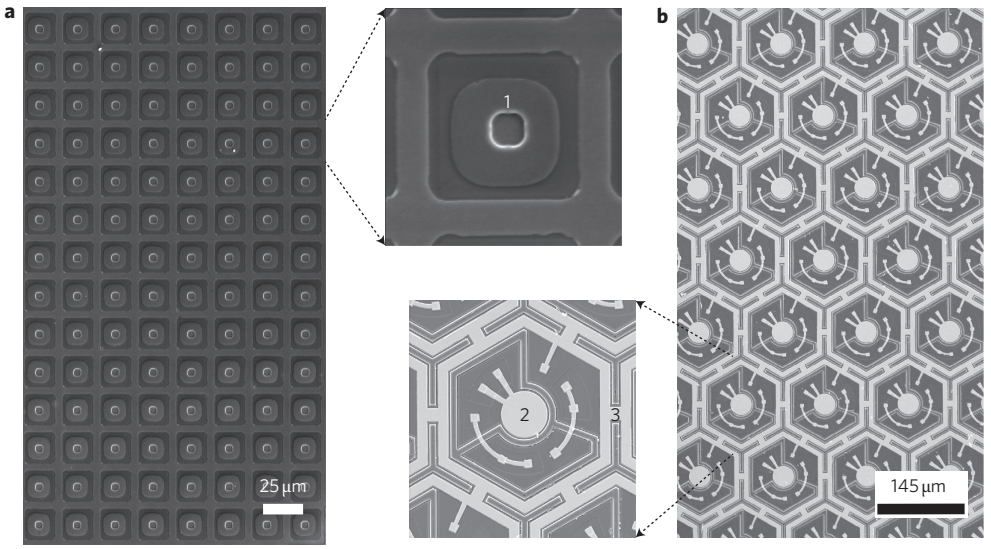

Figure 2 | Subretinal photodiode arrays. a, Photodiode array consisting of 25 μm pixels, each containing a ~10 μm stimulating electrode ('1' in inset) surrounded by the photosensitive area of a single photodiode. The return electrode common to all pixels is situated on the back of the array. **b**, Array with three-diode pixels arranged in a hexagonal pattern. Pixels of 70 and 140 μm in size were made. Central electrodes ('2' in inset) with diameters of 20 and 40 μm, respectively, are surrounded by three diodes connected in series, and by the common return electrode ('3' in inset). Pixels are separated by 5 μm trenches to improve perfusion and for better isolation (140 μm pixel is shown in the inset).

stimulation pattern into bursts of spikes from the retinal ganglion cells (RGCs). This is in contrast to the exact pulse timing required for the direct activation of RGCs in the epiretinal approach.

Ambient light is too dim to produce sufficient photocurrent to directly stimulate neurons, by a factor of at least 1,000 (refs 13,14). We therefore use a NIR laser image projection system that produces pulsed illumination of sufficient intensity to drive the photodiode array, while remaining invisible to any remaining photoreceptors. The pulsed light induces charge-balanced biphasic pulses in the silicon photodiode array, thereby avoiding electrode erosion and hydrolysis[15,16]. However, care must be taken to avoid excessive retinal heating. The light-induced temperature rise must be kept within the physiological range (below 1 °C) as codified in ocular safety regulations[17]. Such thermal considerations limit average retinal irradiances to ~5.2 mW mm^{-2} at the 905 nm wavelength used in this study[18] (for derivation see Methods). In addition to the cumulative effect of chronic exposure, the retina must not overheat during a single pulse. For pulse durations in the range 0.05–70 ms, the limit for peak irradiance is given by the equation $285t^{-0.25}$, where t is the pulse duration in milliseconds and the result is in mW mm^{-2} (see Methods). For example, peak irradiance is limited to 285 mW mm^{-2} for a 1 ms pulse at a wavelength of 905 nm.

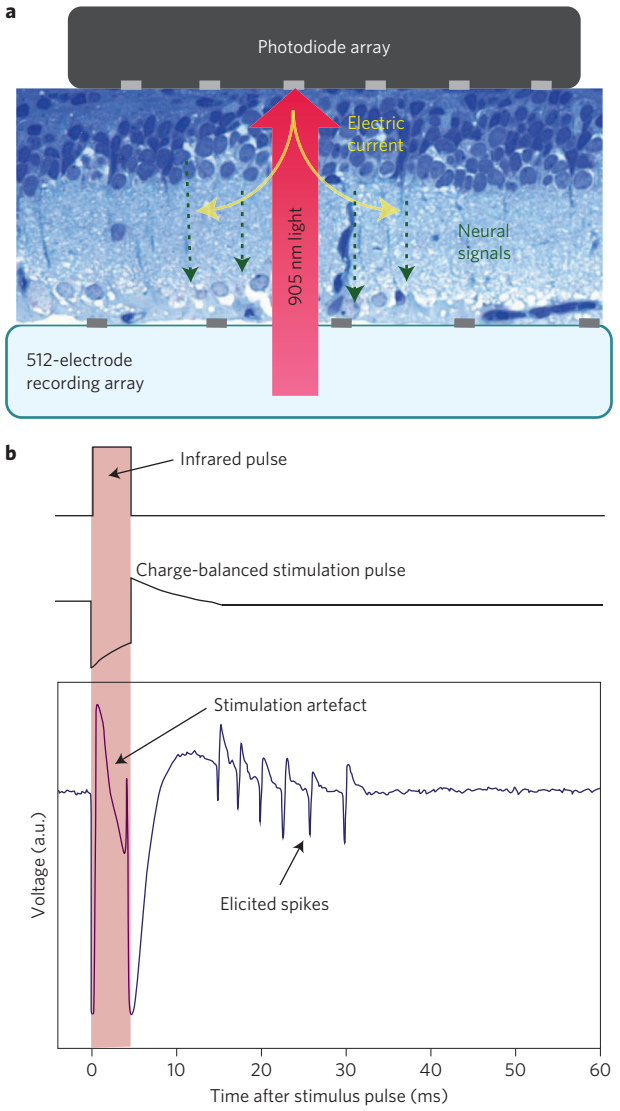

Figure 3 | *In vitro* electrophysiology. a, Schematic of photovoltaic stimulation characterization system. Both healthy and degenerate rat retinas were placed between the stimulating and recording arrays, with the ganglion cell layer facing the recording electrodes. The photodiode array converts patterned 880–905 nm illumination into stimulation currents. **b**, An infrared pulse, with variable pulse width and intensity, creates a charge-balanced current waveform in each pixel of the photodiode array. The microelectrode array records the resultant stimulus artefact and retinal responses from each of the 512 electrodes. Stimulation is repeated at least 400 times for each setting. The artefact is then subtracted and the recorded action potentials undergo principal component analysis and automated clustering to attribute spiking waveforms to over 100 RGCs per experiment.

Initial evaluation of our approach was performed using a photodiode array (ASR, Optobionics[19]) in which each 25 μm pixel contains a photodiode connected to a ~10 μm activated iridium oxide film electrode. Although all pixels share a single large-return electrode located on the back of the ASR, each pixel independently converts locally received light into cathodal-first, charge-balanced pulses (Fig. 2a).

Achieving high spatial resolution may be complicated by the interference of currents from nearby pixels as they travel to the distant return electrode common to all pixels in this array design[12]. One way of reducing such crosstalk is to provide individual local return electrodes for each pixel. Although this solves the problem of crosstalk, it also decreases the penetration depth of electric current into tissue[12]. For this reason and to increase the dynamic range of stimulation, our next-generation devices have local return electrodes and three diodes per pixel, providing a substantially higher current density.

Triple-diode pixels

Single photodiode pixels produce up to 0.5 V at physiologically safe light intensities[12,18]. Both *in vitro*[18] and *in vivo*[9] data indicate that this voltage can successfully stimulate the retina. However, larger voltages can be safely applied in a physiological environment[20–22]. Pixels with three diodes in series can produce 1.5 V, which triples charge injection on the sputtered iridium oxide film electrodes, from 0.5 mC cm^{-2} for a single diode to 1.5 mC cm^{-2} (ref. 18). This increase requires three times higher light intensities, because the photosensitive pixel area is now divided into three subunits. We fabricated implants with 70 and 140 μm pixels containing 20- and 40-μm-diameter stimulation electrodes; the corresponding pixel densities were 178 and 55 pixels/mm^2 (Fig. 2b). All implants were 30 μm thick, to provide sufficient depth for absorption of the NIR light in silicon (penetration depth of 905 nm light in silicon is 35 μm; ref. 23), but thin enough to be implanted subretinally.

Two sizes of arrays were constructed: 0.8 × 1.2 mm for implantation into rats, and 2 × 2 mm for implantation into larger animals. Trenches etched between neighbouring pixels provided electrical isolation, eliminating pixel crosstalk within the silicon device. Each pixel was provided with a local return electrode to constrain stimulation currents to nearby neurons, improving the achievable resolution of the prosthetic device.

Electrophysiological testing

The responses of six healthy and five degenerate[11] (RCS, Royal College of Surgeons) rat retinas were tested under subretinal photovoltaic stimulation by recording RGC spikes induced by NIR stimuli. A schematic of the experimental set-up is shown in Fig. 3a. Briefly, we placed an isolated retina between the photodiode array and a multielectrode array (MEA) consisting of 512 electrodes spaced by 60 μm (ref. 24), with the RGCs facing the recording electrodes. The photodiode array receives pulses of patterned NIR light projected through the transparent MEA and retina, and converts it to electrical currents. Spontaneous RGC spiking was recorded by the MEA and compared with RGC activity during the application of infrared and visible light (spatiotemporal white noise) stimulation, in the same preparation. The data were subject to subtraction of the stimulation artefact and a neuron identification procedure[24–27], resulting in the detection of spike trains from individual RGCs. The data analysis is outlined in more detail in Supplementary Fig. S1.

The area of the MEA was 1.7 mm^2, over which 100 individual neurons were typically detected. In the healthy wild-type rat retina, we observed reliable responses to NIR flashes with a pulse width of 0.5–4 ms. Without the photodiode arrays, the retinal neurons did not respond to NIR light. The majority of neurons responded with latencies of 10–70 ms, although some neurons also exhibited responses with latencies in the 2–5 ms range. Following application of neurotransmitter blockers DNQX (70 μM) and L-AP7 (200 μM), both groups of spikes disappeared, indicating that these responses were elicited by stimulation of the inner retina. Reliable identification of the sub-5 ms spiking was challenging because of the strong stimulus artefact, so we excluded the sub-5 ms latency responses from the subsequent quantitative analysis.

The single- and triple-diode devices elicited very similar responses. Figure 4a,b describes a representative peristimulus time histogram of the RGC response of a healthy retina to NIR flashes of different peak irradiances and durations for the 140 μm

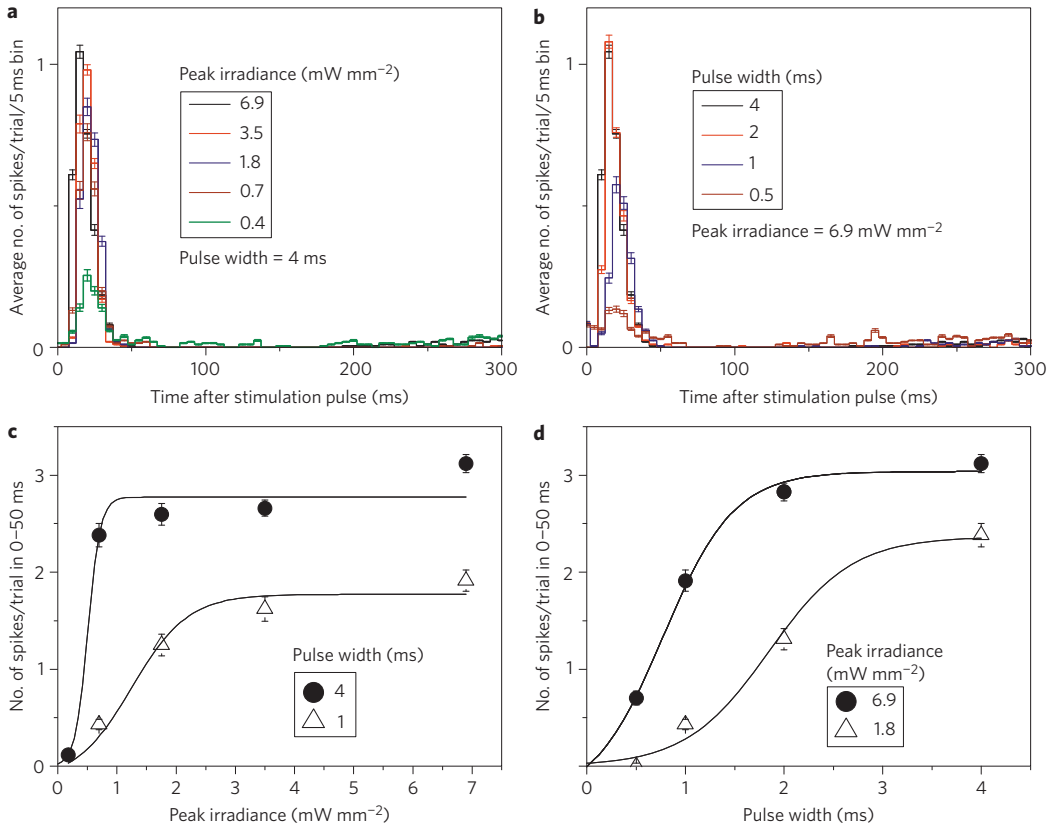

Figure 4 | Stimulation of healthy retina. a,**b**, Peristimulus time histograms showing the stimulated response of a wild-type rat retina, using triple-diode devices, to different peak irradiances at a fixed pulse width of 4 ms (**a**) and for various pulse widths at a fixed irradiance of 6.9 mW mm^{-2} (**b**). **c**, Increase of retinal response with peak irradiance for two pulse widths. **d**, Increase of retinal response with pulse width for two peak irradiances. Error bars denote standard error of the mean.

triple-diode pixels. The change in the average number of elicited spikes with the duration and peak intensity of the NIR flashes (Fig. 4c,d) shows that varying either parameter can modulate the retinal response. The strength–duration dependence of the stimulation threshold (defined as a 50% probability of eliciting a spike) is shown in Fig. 5e,f, with the standard deviation shown as a shaded area. With the 140 μm three-diode devices, the threshold for 1 ms pulses was 0.9 ± 0.2 mW mm^{-2}, decreasing to 0.3 ± 0.1 mW mm^{-2} for 4 ms pulses. For the single-diode devices, the stimulation threshold for wild-type retina was 0.8 ± 0.4 mW mm^{-2} with 1 ms pulses, decreasing to 0.2 ± 0.1 mW mm^{-2} with 4 ms pulses (Supplementary Fig. S2). These results were obtained using full-field illumination of the implants. All error bars in Figs 4 and 5a–d denote the standard error of the mean.

To check whether the observed RGC responses resulted from photoreceptor activation by the electric currents, we selectively blocked synaptic transmission from photoreceptors to ON bipolar cells with L-AP4 (an mGluR6 receptor agonist, 100 μM). As expected, application of L-AP4 led to the disappearance of visible light responses in ON-centre but not OFF-centre RGCs, as assessed from the spike-triggered average of the RGC responses to the visible spatiotemporal white noise stimulus[24–27]. In contrast, the responses of the ON-centre RGCs to electrical stimulation were unchanged, indicating that the stimulation is most probably not due to the photoreceptors themselves, but rather due to activation of the subsequent neuronal layers (see Supplementary Fig. S3 for more details).

Degenerating retina is known to undergo significant anatomical restructuring[28,29]. We tested the effect of this degeneration on photovoltaic subretinal stimulation by performing similar experiments on RCS rat retinas 60 to 90 days postnatal, when the vast majority of photoreceptors have degenerated. Again, we were able to record from ~100 neurons in each preparation, with all five data sets showing clear stimulation with a similar spatial distribution to that observed in wild-type RGCs. Figure 5a–d shows a typical response of one of the RGCs to NIR flashes of various durations and intensities (data for a triple-diode device). Supplementary Fig. S2 shows the corresponding data for single-diode devices. Figure 5e,f shows the strength–duration dependencies of the mean RGC stimulation thresholds for wild-type ($N = 15$) and RCS ($N = 24$) retinas activated by single-diode (Fig. 5e) and triple-diode (Fig. 5f) devices. The RCS retinal stimulation thresholds with triple-diode devices were approximately two to three times higher than in the wild-type; with single-diode devices this ratio increased to up to six. For example, the 1 ms RCS stimulation threshold was 2 mW mm^{-2} with triple-diode devices, but 5 mW mm^{-2} with single-diode devices. At 4 ms the thresholds decreased to 0.8 mW mm^{-2} for both the triple- and single-diode devices. The observed thresholds are about two orders of magnitude below ocular safety limits for both peak and average power (Fig. 5e,f).

In all data sets, the retinal responses contained spike bursts where the number of spikes increased with both irradiance and pulse width, with a mean latency of ~25 ms in wild-type retinas and ~35 ms in RCS retinas. Bursts of spikes lasted ~40 ms after the stimulus in wild-type retinas and 60 ms in RCS retinas. For the single-diode monopolar devices, the maximum number of spikes in the burst saturated at approximately four in wild-type retina and three in RCS. The triple-diode devices were able to elicit

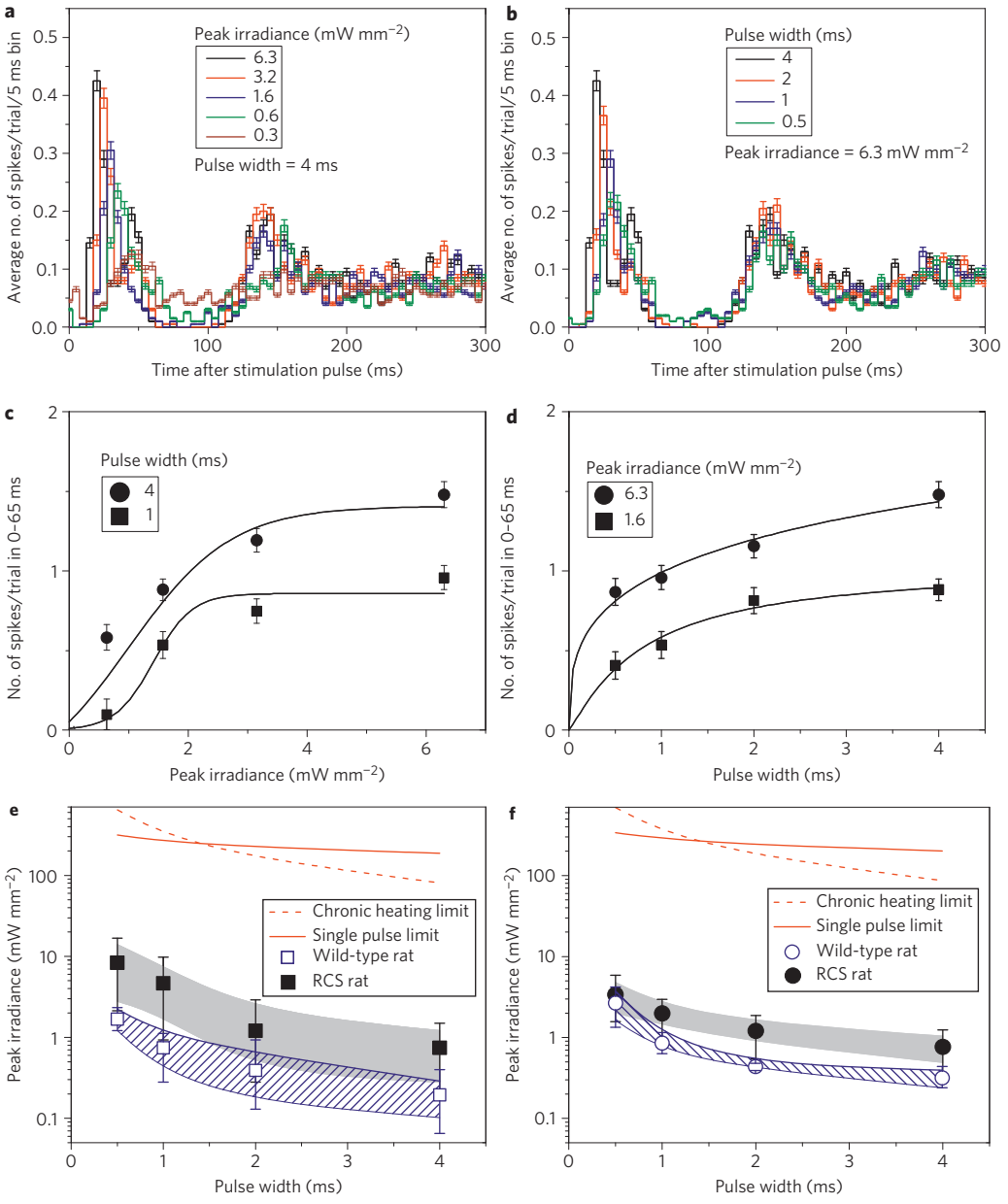

Figure 5 | Stimulation of degenerate retina and strength-duration data. a,**b**, Peristimulus time histograms showing the elicited response of RCS rat retina, using triple-diode devices, at a fixed NIR pulse width (**a**) and at a fixed light intensity (**b**). **c**,**d**, The number of elicited spikes increases with irradiance (**c**) and with pulse width (**d**). **e**, Strength–duration plot for both wild-type and RCS rat retinas, showing the average stimulation thresholds for 10 neurons in both healthy and degenerate retinas with single-diode devices. **f**, Average threshold values for triple-diode devices are plotted for six neurons in two preparations (wild-type) and 14 neurons in a single preparation (RCS). In **e** and **f**, shaded and hashed areas represent the range of standard deviation, and bars indicate the minimum and maximum for each data point. The optical safety limits for a single-pulse and continuous retinal illumination (15 Hz repetition rate) with 905 nm light are also plotted. Error bars in **a**–**d** denote standard error of the mean.

bursts of up to three spikes in wild-type and RCS retinas for the irradiance values shown. However, bursts of up to seven spikes could be elicited in both wild-type and RCS retinas with longer pulse durations and higher irradiance, illustrating the extended dynamic range of the triple-diode devices.

In wild-type retinas the firing rate increased from a spontaneous background of ~3 Hz to over 100 Hz for a brief period (10–50 ms) after the pulse. In the degenerate retina the spontaneous rate of RGC activity is known to be higher[30] and it increased from ~15 Hz to 85 Hz within a time window of 10–65 ms after photovoltaic stimulation.

RGC activity was elicited from an RCS retina with a NIR light spot size as small as $60 \times 60\ \mu m$ with a threshold of 2.7 mW mm^{-2} using 4 ms pulses on the single-diode device. Illuminating a single 140 μm triple-diode pixel elicited RCS retinal activity with a threshold of 4.1 mW mm^{-2} for a pulse duration of 4 ms. Similarly, illuminating a single 70 μm triple-diode pixel for 4 ms at 4.9 mW mm^{-2} elicited a threshold retinal response.

Discussion

Figures 3 and 4 demonstrate that elicited RGC responses can be modulated by both light intensity and pulse width. The described optical system uses a liquid crystal display (LCD) illuminated by a laser beam to form patterns of NIR light (see description in the Methods), enabling only intensity modulation within each video

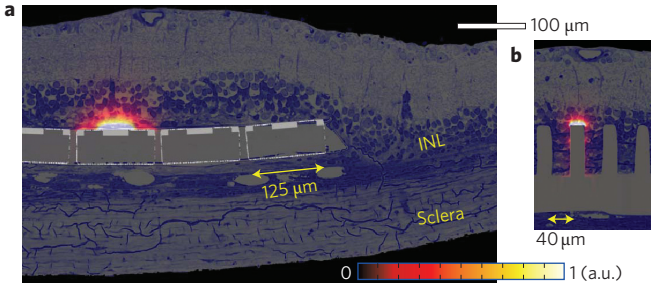

Figure 6 | Pillar arrays for improved proximity. a, Retinal histology of a flat polymer implant in the subretinal space of an RCS rat, with the numerically calculated current distribution from a 115 μm pixel (pixel schematics overlaid). **b**, Retinal histology of a pillar array implant, overlaid with the numerically calculated current distribution from electrodes placed on top. Implants with pixel densities greater than 256 pixels/mm^2 will probably require the use of such three-dimensional geometries to achieve sufficient proximity to target neurons.

frame. However, as the retinal response can also be modulated by varying the pulse width, DLP technology (Texas Instruments) based on an array of high-speed actuated micromirrors can also be used[31]. Such a device would allow both the duration and timing of exposure to be precisely controlled on the scale of individual pixels. In addition to higher throughput compared to an LCD, this high-speed control would allow the sequential activation of nearby pixels to further reduce pixel crosstalk.

The full-field stimulation thresholds were more than two orders of magnitude below the ocular safety limit and were determined using cathodal-first stimulation pulses. Thresholds for single pixel stimulation were more than one order of magnitude below the ocular safety limits. This could perhaps be lowered, by a factor of between two and seven, if anodal-first pulses were to be used[32]. Our fabrication process can be easily altered to accommodate the opposite polarity.

As stimulation thresholds rapidly increase with distance to the target cells[12,33], high-resolution retinal stimulation requires close electrode–neuron proximity—apposition on the order of the size of the stimulating electrode[12]. To assess the proximity of the inner retinal neurons to subretinal implants we fabricated 30-μm-thick (matching our active devices) polymer (Microchem SU8) implants that can be sectioned together with tissue for histology. These devices were coated with SIROF to match our electrode material and implanted in the subretinal space of RCS rats for six weeks[34]. The histological section of an RCS rat retina shown in Fig. 6a demonstrates that the INL is separated from the implant surface by 5–25 μm. Electric current must penetrate at least this depth to ensure effective neural stimulation.

We have computed the current density distribution from single pixels of various dimensions with the COMSOL Conductive Media DC package, where the retina is modelled as a resistive medium. Figure 6a presents the current density in front of a 115 μm pixel with a 40 μm active electrode and circumferential returns, superimposed on a histological section of a flat implant in the subretinal space of an RCS rat. The current penetrates sufficiently deeply to provide targeted stimulation of many neurons in the INL. However, smaller, 62 μm pixels with 20 μm active electrodes can affect fewer such neurons, and will probably require either increased light intensity or improved proximity for effective stimulation.

We have previously shown that retinal cells migrate inside and around three-dimensional subretinal implants, an effect that may be used to achieve intimate neuron–electrode proximity[35]. The histological section in Fig. 6b depicts an array of 15-μm-diameter, 65-μm-tall pillars six weeks after implantation. The bipolar cells surround the pillar tops, placing them in cellular-scale proximity to the tips of the pillar electrodes. The computed current distribution for this geometry overlies the histological section, demonstrating that such pillar arrays can effectively deliver stimulation currents to the INL, and could provide a mechanism for reducing the thresholds and improving stimulation localization in future devices.

Finally, the need to conform to eye curvature inherently limits the sizes of rigid implants to at most a few millimetres. The use of a flexible silicon substrate[36] can overcome this limitation and allow larger arrays to deform elastically to the curvature of the eye. Trenches etched between neighbouring pixels lead to 0.5-μm-thin silicon 'springs' (Supplemental Fig. S4a,b). Optical coherence tomography shows a 6-mm-wide sample array with 75 μm pixels conforming to the curvature of a pig retina (Supplemental Fig. S4c), despite its very large size, a feat made possible by the inherent two-dimensional deformability of the flexible silicon mesh.

Because the photovoltaic implant is thin and wireless, the surgical procedure is much simpler than in other retinal prosthetic approaches. As in conventional subretinal surgery, the procedure involves a partial vitrectomy followed by a subretinal injection to create a retinal bleb. The implant is then inserted into the subretinal space through a retinal incision, and the retina is reattached[19]. As large incisions can complicate retinal reattachment, retinotomies should be as small as practically possible. All pixels in the implant function independently, so several smaller arrays may be inserted through the same retinotomy to tile a large area.

In conclusion, we demonstrate that NIR light-induced photovoltaic stimulation using a subretinal photodiode array elicits bursts of RGC spikes in both healthy and degenerate rat retinas at irradiances substantially below ocular safety limits. The response can be modulated by either pulse duration or irradiance in each pixel. Such a fully integrated wireless implant promises the restoration of useful vision to patients blinded by degenerative retinal diseases.

Methods

Infrared projection system. As LEDs cannot meet the brightness requirement of our implant[12], the infrared projection system made use of an array of laser diodes coupled into a multimode fibre to produce high-intensity illumination with reduced coherence. A microlens array diffuser was used to improve homogeneity and introduce a 5° angular spread to the collimated beam. Speckling at the image plane was measured to be less than 1% (standard deviation). An ocular lens was used to image a transmissive LCD panel onto the retina, similar to conventional video goggles but with ~1,000 times greater peak brightness[12].

Triple-diode pixels. The triple-diode pixel photovoltaic arrays shown in Fig. 5 were manufactured on silicon-on-insulator wafers using a six-mask lithographic process. Light absorbed in the silicon was converted into a charge-balanced biphasic pulse of electric current flowing through the tissue between the active and return electrodes[18]. (A detailed discussion of the fabrication technique is to be published elsewhere.)

Multi-electrode array recordings. Electrophysiological experiments began with enucleation of the eye from an anaesthetized (35 mg kg^{-1} ketamine, 5 mg kg^{-1} xylazine, 0.01 mg kg^{-1} glycopyrrolate) rat, which was subsequently euthanized. A small piece of retina (~3 mm × 3 mm) was isolated and placed between the recording array (ganglion cell side) and the photodiode array (photoreceptors side), as shown in Fig. 2. The retina was perfused with Ames' solution bubbled with 95% oxygen and 5% carbon and kept at 25–30 °C. At least 400 NIR pulses were applied for each parameter setting at a repetition rate of 2 Hz. Recorded voltage waveforms from each of the 512 electrodes were analysed with the spike-finding software described previously[24–27]. We calculated the stimulation threshold as the irradiance required for 50% spike initiation efficiency, that is, eliciting on average one spike for every two stimuli. Experiments were performed on five healthy wild-type rats and four RCS rats, which model retinal degeneration[11]. All experimental procedures were conducted in accordance with institutional guidelines and conformed to the guidelines of the Association for Research in Vision and Ophthalmology (ARVO) Statement for the Use of Animals in Ophthalmic and Vision Research.

Optical safety considerations. NIR light (880–905 nm) is absorbed primarily by pigmented tissues such as the retinal pigment epithelium, with a practically negligible absorption coefficient (<0.06 cm^{-1}) in transparent ocular layers such as the cornea, lens and neural retina. According to ocular safety standards[37,38], the maximum permissible radiant power (MPΦ) that may be delivered chronically to

the retina is $MP\Phi = 6.93 \times 10^{-5}\, C_T C_E P^{-1}$, where $C_T = 10^{0.002(\lambda-700)}$ in the 700–1,050 nm range, with $C_T = 2.5$ at $\lambda = 905$ nm. C_E depends on the angular spread of the incident beam and for retinal spot sizes greater than 1.7 mm in diameter is 29.3 W mm^{-2}. P is the pupil factor, which models pupil constriction or dilation, and is exactly one for infrared wavelengths in the absence of dilating drugs. For the 905 nm wavelength used in this study the average irradiance limit is 5.2 mW mm^{-2}. For single-pulse exposure, the peak irradiance limit in the 0.05–70 ms duration range is described by the equation[30,31] $MP\Phi = 6.93 \times 10^{-4} C_T C_E t^{-0.25}$, where t is in seconds. At 905 nm, $MP\Phi = 285 t^{-0.25}$, where t is in milliseconds and the result is in mW mm^{-2}. Both the chronic limit and the single pulse limit are plotted in Fig. 5e,f as a function of pulse duration, assuming a pulse repetition rate of 15 Hz.

Temperature rise during *in vitro* stimulation. Light incident on a photovoltaic prosthesis produces heat, resulting in a small temperature rise in the retina. NIR light has a penetration depth in silicon on the order of 30 μm (ref. 23), and the temperature rise by the end of a 1 ms pulse at an irradiance of 1 mW mm^{-2} does not exceed 0.002 °C (for a 30-μm-thick device in water). With a repetition rate of 2 Hz, corresponding to a duty cycle of 0.2%, the average temperature rise of a device during prolonged irradiation in a perfused chamber is even lower. Such a minute temperature rise cannot elicit neural stimulation, nor damage tissue.

Received 4 January 2012; accepted 4 April 2012; published online 13 May 2012

References

1. Smith, W. *et al.* Risk factors for age-related macular degeneration: pooled findings from three continents. *Ophthalmology* **108,** 697–704 (2001).
2. Haim, M. Epidemiology of retinitis pigmentosa in Denmark. *Acta Ophthalmol. Scand.* (Suppl) **233,** 1–34 (2002).
3. Kim, S. Y. *et al.* Morphometric analysis of the macula in eyes with disciform age-related macular degeneration. *Retina* **22,** 471–477 (2002).
4. Mazzoni, F., Novelli, E. & Strettoi, E. Retinal ganglion cells survive and maintain normal dendritic morphology in a mouse model of inherited photoreceptor degeneration. *J. Neurosci.* **28,** 14282–14292 (2008).
5. Stone, J. L., Barlow, W. E., Humayun, M. S., de Juan, E. Jr & Milam, A. H. Morphometric analysis of macular photoreceptors and ganglion cells in retinas with retinitis pigmentosa. *Arch. Ophthalmol.* **110,** 1634–1639 (1992).
6. Ahuja, A. K. *et al.* Blind subjects implanted with the Argus II retinal prosthesis are able to improve performance in a spatial-motor task. *Br. J. Ophthalmol.* **95,** 539–543 (2010).
7. Zrenner, E. *et al.* Subretinal electronic chips allow blind patients to read letters and combine them to words. *Proc. R. Soc. B* **278,** 1489–1497 (2010).
8. Besch, D. *et al.* Extraocular surgery for implantation of an active subretinal visual prosthesis with external connections: feasibility and outcome in seven patients. *Br. J. Ophthalmol.* **92,** 1361–1368 (2008).
9. DeMarco, P. *et al.* Stimulation via a subretinally placed prosthetic elicits central activity and induces a trophic effect on visual responses. *Invest. Ophthalmol. Vis. Sci.* **48,** 916–926 (2007).
10. Pardue, M. *et al.* Possible sources of neuroprotection following subretinal silicon chip implantation in RCS rats. *J. Neural Eng.* **2,** S39–S47 (2005).
11. Bourne, M. C., Campbell, D. A. & Tansley, K. Hereditary degeneration of the rat retina. *Br. J. Ophthalmol.* **22,** 613–623 (1938).
12. Loudin, J. D. *et al.* Optoelectronic retinal prosthesis: system design and performance. *J. Neural Eng.* **4,** S72–S84 (2007).
13. Palanker, D. V. *et al.* Design of a high-resolution optoelectronic retinal prosthesis. *J. Neural Eng.* **2,** S105–S120 (2005).
14. Stelzle, M., Stett, A., Brunner, B., Graf, M. & Nisch, W. Electrical properties of micro-photodiode arrays for use as artificial retina implant. *Biomed. Microdev.* **3,** 133–142 (2001).
15. Brummer, S. B. & Turner, M. J. Electrical-stimulation of nervous-system—principle of safe charge injection with noble-metal electrodes. *Bioelectrochem. Bioenerg.* **2,** 13–25 (1975).
16. Cogan, S. F., Guzelian, A. A., Agnew, W. F., Yuen, T. G. & McCreery, D. B. Over-pulsing degrades activated iridium oxide films used for intracortical neural stimulation. *J. Neurosci. Methods* **137,** 141–150 (2004).
17. Active Implantable Medical Devices, in *Directive 90/385/EEC*; available at http://ec.europa.eu/enterprise/policies/european-standards/harmonised-standards/implantable-medical-devices/ (2004).
18. Loudin, J., Cogan, S., Mathieson, K., Sher, A. & Palanker, D. Photodiode circuits for retinal prostheses. *IEEE Trans. Biomed. Circ. Syst.* **5,** 468–480 (2011).
19. Chow, A. *et al.* The artificial silicon retina microchip for the treatment of vision loss from retinitis pigmentosa. *Arch. Ophthalmol.* **122,** 460–469 (2004).
20. Beebe, X. & Rose, T. Charge injection limits of activated iridium oxide electrodes with 0.2 ms pulses in bicarbonate buffered saline (neurological stimulation application). *IEEE Trans. Biomed. Eng.* **35,** 494–495 (1988).
21. Cogan, S., Troyk, P., Ehrlich, J., Plante, T. & Detlefsen, D. Potential-biased, asymmetric waveforms for charge-injection with activated iridium oxide (AIROF) neural stimulation electrodes. *IEEE Trans. Biomed. Eng.* **53,** 327–332 (2006).
22. Negi, S., Bhandari, R., Rieth, L., Van Wagenen, R. & Solzbacher, F. Neural electrode degradation from continuous electrical stimulation: comparison of sputtered and activated iridium oxide. *J. Neurosci. Methods* **186,** 8–17 (2010).
23. Green, M. A. & Keevers, M. J. Optical properties of intrinsic silicon at 300 K. *Prog. Photovoltaics* **3,** 189–192 (1995).
24. Litke, A. M. *et al.* What does the eye tell the brain?: development of a system for the large-scale recording of retinal output activity. *IEEE Trans. Nucl. Sci.* **51,** 1434–1440 (2004).
25. Field, G. D. *et al.* High-sensitivity rod photoreceptor input to the blue-yellow color opponent pathway in macaque retina. *Nature Neurosci.* **12,** 1159–1164 (2009).
26. Field, G. D. *et al.* Spatial properties and functional organization of small bistratified ganglion cells in primate retina. *J. Neurosci.* **27,** 13261–13272 (2007).
27. Petrusca, D. *et al.* Identification and characterization of a Y-like primate retinal ganglion cell type. *J. Neurosci.* **27,** 11019–11027 (2007).
28. Jones, B. W. & Marc, R. E. Retinal remodeling during retinal degeneration. *Exp. Eye Res.* **81,** 123–137 (2005).
29. Jones, B. W. *et al.* Retinal remodeling triggered by photoreceptor degenerations. *J. Comp. Neurol.* **464,** 1–16 (2003).
30. Pu, M., Xu, L. & Zhang, H. Visual response properties of retinal ganglion cells in the Royal College of Surgeons dystrophic rat. *Invest. Ophthalmol. Vis. Sci.* **47,** 3579–3585 (2006).
31. Hornbeck, L. J. Digital light processing for high-brightness, high-resolution applications (invited paper). *Proc. SPIE Projection Disp. III* **3013,** 27–40 (1997).
32. Jensen, R. J. & Rizzo, J. F. Thresholds for activation of rabbit retinal ganglion cells with a subretinal electrode. *Exp. Eye Res.* **83,** 367–373 (2006).
33. Sekirnjak, C. *et al.* High-resolution electrical stimulation of primate retina for epiretinal implant design. *J. Neurosci.* **28,** 4446–4456 (2008).
34. Butterwick, A. *et al.* Effect of shape and coating of a subretinal prosthesis on its integration with the retina. *Exp. Eye Res.* **88,** 22–29 (2009).
35. Palanker, D. *et al.* Migration of retinal cells through a perforated membrane: implications for a high-resolution prosthesis. *Invest. Ophthalmol. Vis. Sci.* **45,** 3266–3270 (2004).
36. Dinyari, R., Rim, S.-B., Huang, K., Catrysse, P. B. & Peumans, P. Curving monolithic silicon for nonplanar focal plane array applications. *Appl. Phys. Lett.* **92,** 091114 (2008).
37. American National Standard for Safe Use of Lasers (ANSI 136.1). ANSI. Vol. ANSI 136.1-2000 (The Laser Institute of America, 2000).
38. DeLori, F., Webb, R. & Sliney, D. Maximum permissable exposures for ocular safety (ANSI 2000), with emphasis on ophthalmic devices. *J. Opt. Soc. Am. A* **24,** 1250–1265 (2007).

Acknowledgements

The authors thank Optobionics, especially G. McLean, for providing the ASR samples, and P. Peumans and R. Dinyari from the Electrical Engineering Department at Stanford University for providing a sample of the flexible silicon grid[36] for tests of its flexibility in a porcine eye. We also thank A.M. Litke, S. Kachiguine, A. Grillo and W. Dabrowski for the development of the 512-electrode recording system, and M. Krause for his help with retinal preparations. The authors thank M.F. Marmor, M.S. Blumenkranz, R. Gariano and S. Sanislo from the Department of Ophthalmology at Stanford for productive discussions regarding implant design and surgical procedures. Thanks also go to S. Cogan at EIC Labs for fabrication advice and for iridium oxide electrode deposition, M. McCall at the University of Louisville for critical manuscript reading, and M. Pardue at Emory University for advice on subretinal implantations into RCS rats. Funding was provided by the National Institutes of Health (grant no. R01-EY-018608), the Air Force Office of Scientific Research (grant FA9550-04) and a Stanford Bio-X IIP grant. K.M. was supported by an SU2P fellowship as part of an RCUK Science Bridges award. J.L. was supported in part by the National Science Foundation Graduate Research Fellowship programme. A.S. was supported in part by a Burroughs Welcome Fund Career Award at the Scientific Interface.

Author contributions

J.L. and D.P. jointly conceived and designed the pulsed-NIR photovoltaic retinal prosthesis system, and the three-diode pixel devices. K.M., T.K. and J.H. led the fabrication team of L.W. and L.G., with L.W. performing most of the fabrication steps that produced the implant device. A.S. and D.P. conceived the electrophysiology experiments, which were carried out by K.M., J.L., G.G. and R.S. under the guidance of A.S. Data analysis was performed by K.M. and G.G. with direction from A.S. The subretinal implantations and histological analysis was performed by P.H. J.L. wrote the first draft of the paper, with K.M., A.S. and D.P. contributing several sections and extensive edits. The project was organized and coordinated by D.P.

Additional information

The authors declare no competing financial interests. Supplementary information accompanies this paper at www.nature.com/naturephotonics. Reprints and permission information is available online at http://www.nature.com/reprints. Correspondence and requests for materials should be addressed to J.L.